MAGNETIC FIELD OF TUBULAR LINEAR MACHINES WITH DUAL HALBACH ARRAY

Liang Yan[1], [*], Lei Zhang[1], Tianyi Wang[1], Zongxia Jiao[1], Chin-Yin Chen[2], and I-Ming Chen[3]

[1]Beihang University, Beijing 100191, China

[2]Taiwan Ocean Research Institute, Kaohsiung 852, Taiwan, R.O.C.

[3]Nanyang Technological University, Nanyang Ave., 639798, Singapore

Abstract—Permanent magnet (PM) array affects flux field distribution of electromagnetic linear machines significantly. A novel dual Halbach array is proposed in this paper to enhance flux density in air gap, and thus to improve output performance of linear machines. Magnetic field in three-dimensional (3D) space of a tubular linear machine with dual Halbach array is formulated based on Laplace's and Poisson's equations. Numerical result from finite element method is employed to simulate and observe the flux distribution in the machine. A research prototype and a testbed are developed, and experiments are conducted to validate the analytical models. The study is useful for analysis and design optimization of electromagnetic linear machines.

1. INTRODUCTION

Electromagnetic linear machine generates linear motions directly without rotation-to-translation conversion mechanisms, which significantly simplifies system structure and improves system efficiency. It has wide applications in aeronautics [1, 2], transportation [3, 4], medical devices [5, 6] and so on. High flux density in linear machines is extremely important for high-force required applications. The employment of permanent magnets (PMs) offers electromagnetic linear machines a number of distinctive features [7] such as excellent servo characteristics and high power density. Optimized PM array is one effective way to improve flux density in linear machines. Axial and radial magnetization arrays are the two most common arrangements of PMs. Magnet

arrays with alternating magnetization directions are configured in [8] to produce radially directed flux density across the air gap of PM motors. A double-sided slotted torus axial-flux PM motor is designed for direct drive of electric vehicle in [9]. [10] is a good paper that introduces analysis and design of linear machines systematically. It provides a unified framework for several structure topologies. Halbach array is a promising magnet pattern due to its self-shielding property and sinusoidally distributed magnetic field in air space. It is widely applied in linear motor systems. For example, in [11], Halbach-arrayed PMs replace the north-south magnet array in MagPipe pipeline transportation system, and increase the motor propulsion force per Ampere significantly. In [12], PMs in Halbach array configuration are used for levitation, propulsion, and guidance of urban transportation systems, and achieve impressive performance.

In this study, a tubular linear machine with dual Halbach array is proposed to further improve the magnetic flux density and thus the force output. It can not only increase the radial component of flux density which is important for axial force generation, but also decrease the local force radial component which causes vibrations. Based on PM arrangement, magnetic field distribution in the machine is formulated with Laplace's and Poisson's equations analytically. Numerical result from finite element method (FEM) is utilized to analyze and observe flux variation in three-dimensional (3D) space of the machine. Following that, a research prototype and a testbed are developed for experimental purpose. Both numerical and experimental results validate the analytical models. The obtained analytical model could be used for analysis of output performance and control implementation of electromagnetic linear machines with similar structures.

2. STRUCTURE AND WORKING PRINCIPLE

The schematic structure of the tubular linear machine with dual Halbach array is illustrated in Fig. (1a). The mover is composed of several winding phases mounted on the holder. Air core structure is employed for linear relationship between force output and current input that may facilitate motion control of the system. The stator consists of PMs located at both internal and external sides of the windings. Back irons are attached on the two layers of PMs to reduce flux leakage and magnetic energy loss. Magnetization pattern and flux distribution of the dual Halbach array are illustrated in Fig. (1b). The magnetization of the internal and external arrays is not the same. Instead, it is a coordination of two Halbach arrays, specifically, with the same magnetization pattern for radially magnetized PMs and the opposite
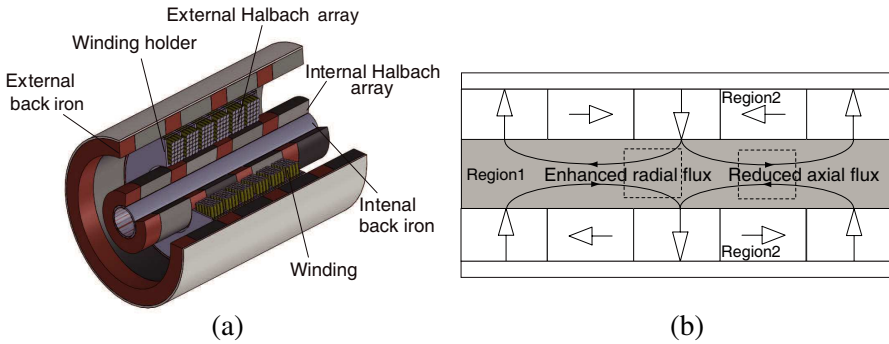
Figure 1. Tubular linear machine with dual Halbach array. (a) Schematic machine structure. (b) Magnetization and flux.

magnetization pattern for axial ones. This special arrangement can increase the radial component of magnetic flux density greatly in the air gap, whereas reduces the axial flux density significantly. It indicates that the dual Halbach array may offer us two advantages, i.e., the axial force can be improved much from the increased radial flux, and the radial force disturbance and vibration can be weakened from the decreased axial flux. The choice of movers (winding or magnets) depends on the requirements of particular applications. In this study, the winding is selected as the mover for the convenience of presentation.

3. GOVERNING EQUATIONS OF FLUX FIELD

Mathematical modeling of magnetic field is important for electromagnetic machines, as it could be used to predict output performance, such as flux linkage, field energy and force generation [13–15]. Generally, there are two typical ways to formulate magnetic field of electromagnetic machines, i.e., FEM [16] and magnetic equivalent circuits [17]. FEM is an efficient and accurate means to calculate magnetic field, taking full account of nonlinearity of iron material and induced currents in electrically conducting parts [18–20]. However, it is time consuming and cannot give much insight into design parameters [21]. Magnetic equivalent circuit can mainly be classified into lumped equivalent circuit and mesh-based one. The lumped equivalent circuit is the simplest approach to model the magnetic field, and allows to establish analytical relationships between design parameters and output performance. However, the technique suffers from inherent inaccuracy especially in presence of complex flux paths [22]. The mesh-based equivalent circuit is developed to achieve higher accuracy through a division of geometry [23]. However, it still requires some computational effort, although

less than FEM, especially for complex models [24]. To obtain accurate knowledge of magnetic fields that directly relate motor geometry and output performance, a more sophisticated analytical field model that can compromise between accuracy and computation time is necessary [25]. Therefore, an analytical field model characterized by series expansions of the solution in terms of harmonic functions is established in this section. It will be validated by both finite element method and experiments. This approach could be applied to field modeling of other electromagnetic machines with similar magnet arrangements, and the derived parametric model is useful for analyzing the influence of parameters on output performance of electric machines.

3.1. Magnetic Characterization of Materials

In formulation of the magnetic field, the machine space under study is divided into two regions based on magnetic characteristics. The air or coil space that has a relative permeability of 1.0 is denoted as Region 1. The PM volume filled with rare-earth magnetic material is denoted as Region 2. The back irons assumed infinite permeability is utilized to reduce magnetic energy loss, and enhance flux density. The magnetic field property of Region 1 and 2 is characterized by the relationship between field intensity, $\mathbf{H}$ (in A/m), and flux density, $\mathbf{B}$ (in Tesla), as

$$\mathbf{B}_1 = \mu_0\mathbf{H}_1, \quad \mathbf{B}_2 = \mu_0\mu_r\mathbf{H}_2 + \mu_0\mathbf{M}, \tag{1}$$

where μ_0 is the permeability of free space with a value of $4\pi\times10^{-7}$ H/m, μ_r the relative permeability of permanent magnets, $\mathbf{M} = \mathbf{B}_{rem}/\mu_0$ the residual magnetization vector in A/m, and $\mathbf{B}_{rem}$ the remanence.

3.2. Governing Equations

The governing equations of magnetic field, i.e., Laplace's and Poisson's equations, are significant for the solution of magnetic field. It is known that magnetic field is a solenoid field or source-free field, i.e.,

$$\nabla \cdot \mathbf{B}_i = 0, \tag{2}$$

where $i = 1$, 2. It can be proved that for any vector, the divergence of its curl is always equal to zero. Thus, we can have a magnetic vector potential, $\mathbf{A}_i$, so that

$$\mathbf{B}_i = \nabla \times \mathbf{A}_i. \tag{3}$$

Because the curl of any function's (f) gradient is always equal to zero, we could have

$$\nabla \times \mathbf{A}_i = \nabla \times (\mathbf{A}_i + \nabla f),$$

which indicates that $\mathbf{A}_i$ may have multiple solutions. To uniquely determine its value, Coulomb gauge, $\nabla \cdot \mathbf{A}_i = 0$, applies as constraint. Under Coulomb gauge, we could have

$$\nabla \times \mathbf{B_i} = -\nabla^2 \mathbf{A}_i. \tag{4}$$

3.2.1. Laplace's Equation for Region 1

The combination of Maxwell's equations and Eq. (1) gives

$$\nabla \times \mathbf{B}_1 = \nabla \times \mu_0 \mathbf{H}_1 = \mu_0 \mathbf{J}. \tag{5}$$

Substituting Eq. (4) into (5) yields

$$\nabla^2 \mathbf{A}_1 = -\mu_0 \mathbf{J},$$

where $\mathbf{J}$ (A/m2) is current density in the field. In this study, $\mathbf{J} = 0$. Therefore, the Laplace's equation for Region 1 is obtained as

$$\nabla^2 \mathbf{A}_1 = 0. \tag{6}$$

3.2.2. Poission's Equation for Region 2

The combination of Maxwell's equations and Eq. (1) gives

$$\nabla \times \mathbf{B}_2 = \mu_0 \mu_r \mathbf{J} + \mu_0 \nabla \times \mathbf{M}. \tag{7}$$

Similarly, Eqs. (4) and (7) yield the Poisson equation for Region 2

$$\nabla^2 \mathbf{A}_2 = -\mu_0 \nabla \times \mathbf{M}. \tag{8}$$

4. GENERAL SOLUTIONS TO MAGNETIC FIELD

4.1. General Solution to Laplace Equation

The magnetic field distribution of tubular linear machine is axially symmetric. Therefore, $\mathbf{A}_i$ has only one component, $A_{i,\theta}$. The Laplace equation in cylindrical coordinators can be simplified as

$$\frac{\partial^2 A_\theta}{\partial z^2} + \frac{\partial}{\partial r}\left(\frac{1}{r}\frac{\partial}{\partial r}(rA_\theta)\right) = 0. \tag{9}$$

Since A_θ is only a function of r and θ, we assume that

$$A_\theta = R(r) Z(z). \tag{10}$$

Substituting into Eq. (9) yields

$$\frac{1}{R(r)}\frac{\partial^2 R(r)}{\partial r^2} + \frac{1}{R(r)r}\frac{\partial R(r)}{\partial r} + \frac{1}{Z(z)}\frac{\partial^2 Z(z)}{\partial z^2} - \frac{1}{r^2} = 0, \tag{11}$$

where r and z are independent variables, and the third term as a function of z must be a constant. So the following formula is established

$$\frac{1}{Z(z)}\frac{\partial^2 Z(z)}{\partial z^2} = k^2. \tag{12}$$

Then Eq. (11) becomes

$$\frac{1}{R(r)}\frac{\partial^2 R(r)}{\partial r^2} + \frac{1}{R(r)\,r}\frac{\partial R(r)}{\partial r} + k^2 - \frac{1}{r^2} = 0. \tag{13}$$

Eq. (12) can then be rewritten as

$$\frac{\partial^2 Z(z)}{\partial z^2} - k^2 Z(z) = 0. \tag{14}$$

Thus, Laplace equation, Eq. (9), is separated into two equations, Eqs. (13) and (14). There are three possible solutions to Eqs. (13) and (14) according to variation of k.

4.1.1. The First Solution

When $k^2 = 0$, the following equations are obtained

$$Z(z) = E_0 + F_0 z, \quad r^2\frac{\partial^2 R(r)}{\partial r^2} + r\frac{\partial R(r)}{\partial r} - R(r) = 0. \tag{15}$$

The solution to Eq. (15) is

$$A_\theta = R(r) Z(z) = \left(C_0 r + D_0\frac{1}{r}\right)(E_0 + F_0 z). \tag{16}$$

However, as A_θ should be a periodic function of z, Eq. (16) is not the valid solution of A_θ.

4.1.2. The Second Solution

When $k^2 > 0$, the following equation is obtained

$$Z(z) = E_0 e^{kz} + F_0 e^{-kz},$$
$$r^2\frac{\partial^2 R(r)}{\partial r^2} + r\frac{\partial R(r)}{\partial r} + R(r)\left(k^2 r^2 - 1\right) = 0. \tag{17}$$

The solution to Eq. (15) is

$$A_\theta = R(r) Z(z) = [C_0 J_1(kr) + D_0 Y_1(kr)]\left(E_0 e^{kz} + F_0 e^{-kz}\right). \tag{18}$$

Again, because Eq. (18) is not a periodic function of z, it is not the solution of Laplace's equation either.

4.1.3. The Third Solution

When $k^2 < 0$, the following equations are obtained

$$Z(z) = B_0 \cos(mz) + B_1 \sin(mz),$$
$$r^2 \frac{\partial^2 R(r)}{\partial r^2} + r \frac{\partial R(r)}{\partial r} + R(r)\left(k^2 r^2 - 1\right) = 0. \tag{19}$$

The solution to Eq. (19) is

$$A_\theta = \left\{ \begin{array}{l} [C_0 I_1(mr) + D_0 K_1(mr)] \cos(mz) \\ + \\ [E_0 I_1(mr) + F_0 K_1(mr)] \sin(mz) \end{array} \right\}, \tag{20}$$

where m is a real number and defined with $k = jm$. In this case, A_θ is a periodic function of z. It is probably the solution of Laplace's equation. To determine the coefficients in above equation, constraints are needed. Because the axial component of flux density is antisymmetry on $z = 0$, we have $\left. B_z \right|_{z=0} = 0$. Substituting Eq. (20) into Eq. (3) gives

$$C_0 = 0, \quad D_0 = 0.$$

Therefore, the general solution to Laplace's equation is

$$A_\theta = [a_n I_1(mr) + b_n K_1(mr)] \sin(mz), \tag{21}$$

where $a_n = E_0$, $b_n = F_0$.

4.2. General Solution to Poisson Equation

The Poisson equation in cylindrical coordinators is

$$\frac{\partial A_\theta}{\partial z^2} + \frac{\partial}{\partial r}\left(\frac{1}{r}\frac{\partial}{\partial r}(r A_\theta)\right) = -\mu_0 \nabla \times \mathbf{M}. \tag{22}$$

The general solution to the corresponding homogeneous equation of the Poisson equation is

$$A_\theta = \sum_{n=1,2,\dots}^{\infty} [a_n I_1(m_n r) + b_n K_1(m_n r)] \sin(m_n z). \tag{23}$$

To get the solution of Poisson equation, the right side of the equation needs to be substituted by harmonic expansion of magnetization vector. As illustrated in Fig. (1b), the two Halbach arrays in the linear machine are composed of radial and axial magnets. The magnetization vector, $\mathbf{M}$, has two components M_r and M_z in r and z directions respectively. It is given in cylindrical coordinators as

$$\mathbf{M} = M_r \mathbf{e}_r + M_z \mathbf{e}_z. \tag{24}$$

M_r is a non-continuous function with a period of $2\tau_p$, and it can be represented with harmonic expansions as

$$M_r = \sum_{n=1,2\dots}^{\infty} 4\left(B_{rem}/\mu_0\right) \frac{\sin\left[(2n-1)\frac{\pi}{2}\alpha_p\right]}{(2n-1)\pi} \cos\left(m_n z\right), \qquad (25)$$

where $\alpha_p = \frac{\tau_r}{\tau_p}$, τ_p is the pole pitch, τ_r is width of radial magnets, n is a positive integer, and

$$m_n = (2n-1)\pi/\tau_p. \qquad (26)$$

Therefore, the general solution of Poisson equation is obtained

$$A_{2\theta} = \sum_{n=1,2,\dots}^{\infty} \left\{\left[a_{2n}I_1\left(m_n r\right) + b_{2n}K_1\left(m_n r\right)\right]\sin\left(m_n z\right) + S\left(r, z\right)\right\}, \qquad (27)$$

where $S(r, z) = R(r)Z(z)$ is a particular solution of Poisson equation. Substituting $S(r, z)$ into Poisson equation gives

$$\frac{1}{R(r)}\frac{\partial^2 R(r)}{\partial r^2} + \frac{1}{R(r)r}\frac{\partial R(r)}{\partial r} + \frac{1}{Z(z)}\frac{\partial^2 Z(z)}{\partial z^2} - \frac{1}{r^2} = \frac{1}{R(r)Z(z)}P_n\sin\left(m_n z\right), \qquad (28)$$

where $P_n = \frac{4}{\tau_p}B_{rem}\sin\left[(2n-1)\frac{\pi}{2}\alpha_p\right]$. Let $\frac{1}{Z(z)}\frac{\partial^2 Z(z)}{\partial z^2} = -m_n{}^2$. It is simplified as

$$Z(z)=\sin(m_n z), \quad r^2\frac{\partial^2 R(r)}{\partial r^2} + r\frac{\partial R(r)}{\partial r} - R(r)\left(m_n{}^2 r^2 + 1\right) = r^2 P_n. \quad (29)$$

Therefore, the particular solution to Poisson equation is

$$S\left(r, z\right) = R\left(r\right)Z\left(z\right) = \frac{\pi L_1\left(m_n r\right)}{2m_n{}^2}P_n\sin\left(m_n z\right), \qquad (30)$$

where L_1 is the modified Struve functions [26] and appears as special solutions of inhomogeneous Bessel equations. As a result, the general solutions to Laplace and Poisson equations are

$$A_{1\theta} = \sum_{n=1,2,\dots}^{\infty} \left[a_{1n}I_1\left(m_n r\right) + b_{1n}K_1\left(m_n r\right)\right]\sin\left(m_n z\right),$$

$$A_{2\theta} = \sum_{n=1,2,\dots}^{\infty} \left\{\left[a_{2n}I_1\left(m_n r\right) + b_{2n}K_1\left(m_n r\right)\right]\sin\left(m_n z\right) \qquad (31)\right.$$

$$\left. + \frac{1}{2}\frac{\pi L_1\left(m_n r\right)}{m_n{}^2}P_n\sin\left(m_n z\right)\right\}.$$

4.3. Solutions to Flux Density Distribution

From Eqs. (3) and (31), the general solution of flux density is obtained

$$
\begin{aligned}
B_{r1} &= \sum_{n=1,2,\ldots}^{\infty} -m_n \left[a_{1n} I_1(m_n r) + b_{1n} K_1(m_n r) \right] \cos(m_n z), \\
B_{r2}^p &= \sum_{n=1,2,\ldots}^{\infty} -m_n \Bigg\{ \left[a_{2n}^p I_1(m_n r) + b_{2n}^p K_1(m_n r) \right] \cos(m_n z) \\
&\quad + \frac{1}{2} \frac{\pi L_1(m_n r)}{m_n{}^2} P_n \cos(m_n z) \Bigg\}, \\
B_{z1} &= \sum_{n=1,2,\ldots}^{\infty} m_n \left[a_{1n} I_0(m_n r) - b_{1n} K_0(m_n r) \right] \sin(m_n z), \\
B_{z2}^p &= \sum_{n=1,2,\ldots}^{\infty} m_n \Bigg\{ \left[a_{2n}^p I_0(m_n r) - b_{2n}^p K_0(m_n r) \right] \sin(m_n z) \\
&\quad + \frac{1}{2} \frac{\pi L_0(m_n r)}{m_n{}^2} P_n \sin(m_n z) \Bigg\}.
\end{aligned}
\tag{32}
$$

B_{r1} and B_{z1} represents the radial and axial magnetic field in the winding region, while B_{r2}^p and B_{z2}^p are in magnet regions. The upper script, $p = 1, 2$, represents external and internal PMs respectively.

4.4. Boundary Conditions

Boundary conditions are necessary to determine the specific solutions of magnetic field. In this study, boundary conditions are employed to calculate the coefficients in magnetic flux density, such as a_{in}, b_{in}. The magnetic field follows certain rules along the boundary of two different media. For example, the flux density component perpendicular to the boundary is continuous in two neighboring media, and the tangential component of magnetic intensity is discontinuous by the amount of surface current at the boundary. In this study, surface current is zero. Therefore, the tangential component of magnetic intensity is continuous. The boundary conditions are

$$
\begin{aligned}
&B_{2z}^1|_{r=R_s} = \mu_0 M_z^1, \quad B_{2z}^2|_{r=R_r} = \mu_0 M_z^2, \quad B_{1r}|_{r=R_b} = B_{2r}^1|_{r=R_b}, \\
&H_{1z}|_{r=R_b} = H_{2z}^1|_{r=R_b}, \quad B_{1r}|_{r=R_a} = B_{2r}^2|_{r=R_a}, \quad H_{1z}|_{r=R_a} = H_{2z}^2|_{r=R_a}.
\end{aligned}
\tag{33}
$$

From the boundary conditions, the coefficients in magnetic flux density can be obtained.

## 5. NUMERICAL SIMULATION AND EXPERIMENTS

In this section, a research prototype of the linear machine with dual Halbach array and an experimental apparatus have been developed. The experimental works are conducted on the flux field distribution to validate the derived analytical models. Furthermore, the mathematical field model is compared with numerical results from FEM. Although FEM is time-consuming, its precision is relatively high without significant influence from manufacturing and model simplification. Therefore, it is used to validate the magnetic analytical model and observe the flux variation in machine space. The design parameters and material characteristics used in the numerical computation are consistent with those in experiments. The finite element solutions are obtained by applying a master-slave boundary at the axial boundaries $z = 0$, $z = \tau_p$ and imposing symmetry boundary at $z = 0$. The highest order of harmonics considered in the analytical solutions is 15.

5.1. Prototype and Experimental Apparatus

A tubular linear machine with dual Halbach array is developed for experimental investigation on the magnetic field as shown in Fig. 2. The windings are mounted on the mover that in turn is fixed on the two guiders. The guiders can slide back and forth on the linear bearing. The bearings are installed on the covers of the stator in which the PM array is mounted. The structure of the research prototype are shown in Fig. 3 and design parameters are given in Table 1. The maximum linear stroke is 36 mm. PMs in the machine are sintered NdFeB35 with $B_{rem} = 1.2\,\text{T}$ and $\mu_r = 1.0997$. The radially magnetized PMs are replaced with segments of diametrically magnetized sector PMs for the convenience of manufacturing and cost reduction.
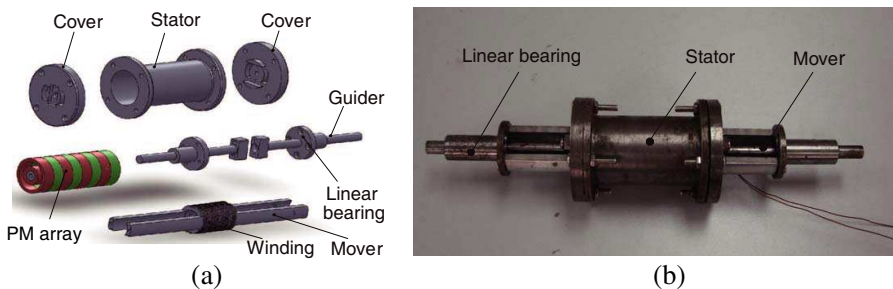
Figure 2. Linear machines with dual Halbach array. (a) 3D exploded view. (b) Research prototype.
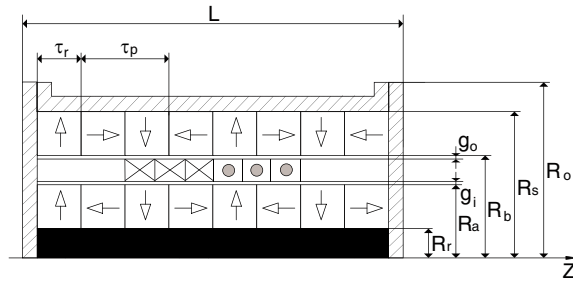
**Figure 3.** Structure of the research prototype.

Table 1. Design parameters of research prototype.

Maximum radius R_o	30 mm	Outer rad of ext PM R_s	17 mm
Machine length L	89 mm	Inner rad of ext PM R_b	14 mm
Width of radial PM τ_r	9 mm	Outer rad of int PM R_a	9 mm
Pole pitch τ_p	18 mm	Inner rad of int PM R_r	5 mm
Number of poles n	4	Number of winding turns	100
Outer air gap g_o	0.2 mm	Inner air gap g_i	0.2 mm

An experimental apparatus is developed for magnetic field measurement in 3D space as illustrated in Fig. 4. The research prototype is mounted on a platform of the apparatus. A gauss probe is installed on the end-effect of a three-axis translational stage. Under the PC controller, the probe can pinpoint to any position inside the linear machine and measure the flux density. The measured data can be either displayed on the Gauss meter or transferred to PC.

5.2. Validation of Analytical Model

In this section, the analytical model of the magnetic field in the linear machine is validated. For winding region, the mathematical model of the flux distribution is compared with both FEM and experimental results. For magnet region, the model is compared with FEM results, as the probe cannot measure the flux field at this region. The numerical model is built in Ansoft environment, using 2D-FEM. Design
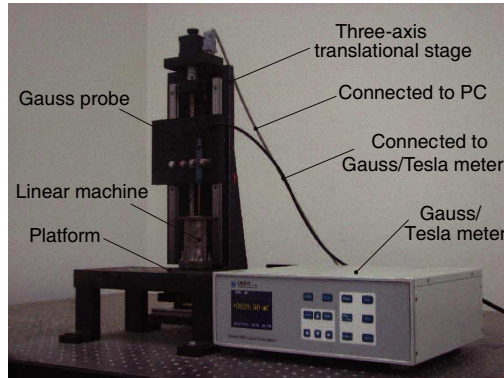
**Figure 4.** Experimental testbed for magnetic field measurement.
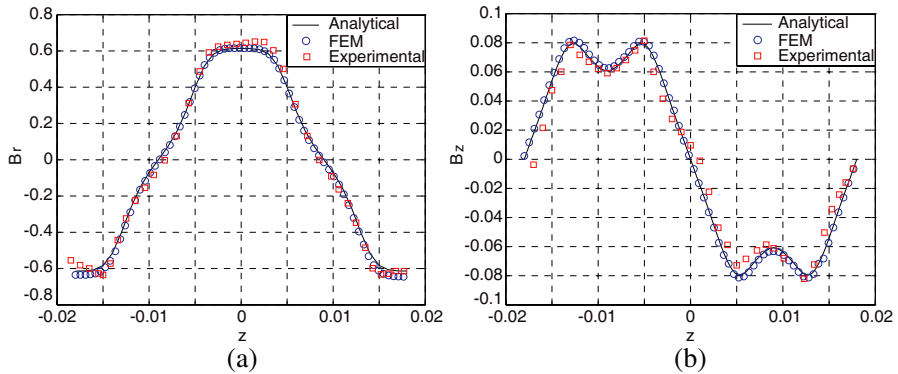
Figure 5. Magnetic field variation versus z at $r = 11.5\,\mathrm{mm}$. (a) B_r variation. (b) B_z variation.

parameters are the same as those in research prototype, and the simulation is implemented by applying master and slave boundary at $z = 0$ and $z = \tau_p$, and symmetry boundary at $z = 0$.

5.2.1. Magnetic Field Variation in Winding Region

Magnetic field variations versus axial distance z are measured and simulated. Results at $r = 11.5\,\mathrm{mm}$, $12\,\mathrm{mm}$, $12.5\,\mathrm{mm}$ are presented in Figs. 5, 6, and 7, respectively. In this study, experiments are conducted neighboring to the center of linear machine ($z = 0$) to reduce the longitude fringe effect. Variation of radial flux component that interacts with current input to produce axial force output is in sine waveform approximately, and harmonic contents of radial flux density at distinctive radius are shown in Fig. 8. It is found that the analytical
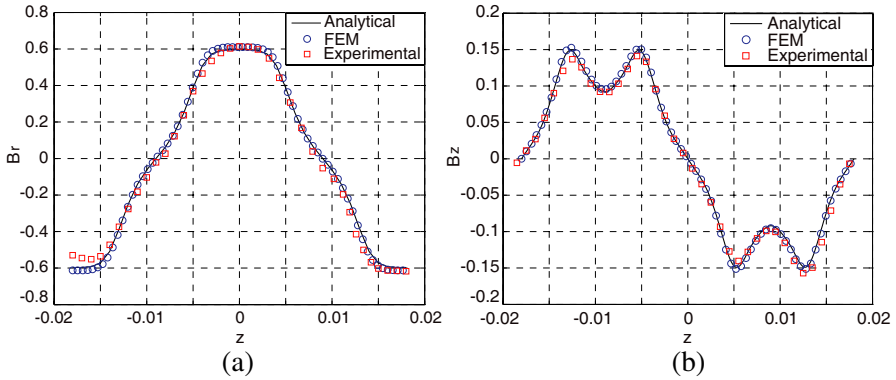
Figure 6. Magnetic field variation versus z at $r = 12\,\text{mm}$. (a) B_r variation. (b) B_z variation.
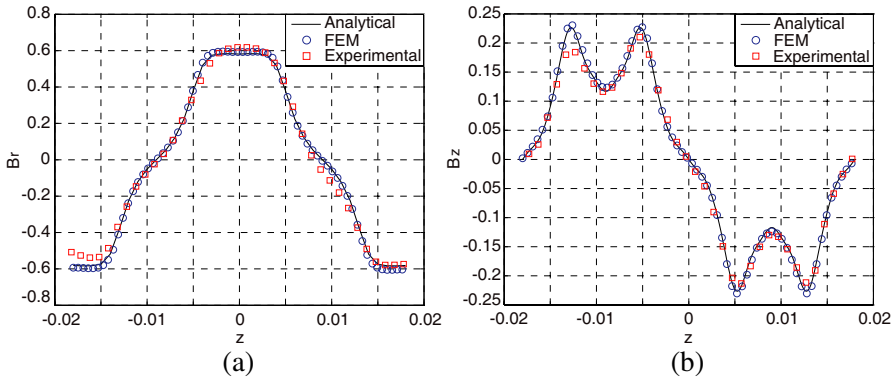

Figure 7. Magnetic field variation versus z at $r = 12.5\,\text{mm}$. (a) B_r variation. (b) B_z variation.

models fit with the finite element results and experimental results closely. The difference is caused by manufacturing errors, assembly errors and replacement of diametrically magnetized segmental PMs.

*5.2.2. Magnetic Field Variation in the Magnet Region*

Figures 9 and 10 present magnetic field variation versus axial distance z at the center radius of internal and external Halbach array, i.e., $r = (R_r + R_a)/2$ and $r = (R_b + R_s)/2$, respectively. Magnetic field in either magnet region varies in line with the magnetization vector **M**. Therefore, the radial flux component is even-symmetric about $z = 0$, while the axial field is odd-symmetric. However, the radial flux density in the internal magnet area is greater than that in the external magnet
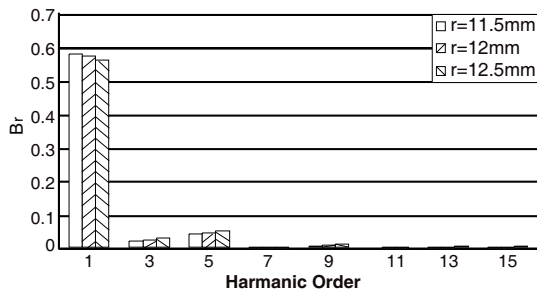
Figure 8. Harmonic content of radial flux density.
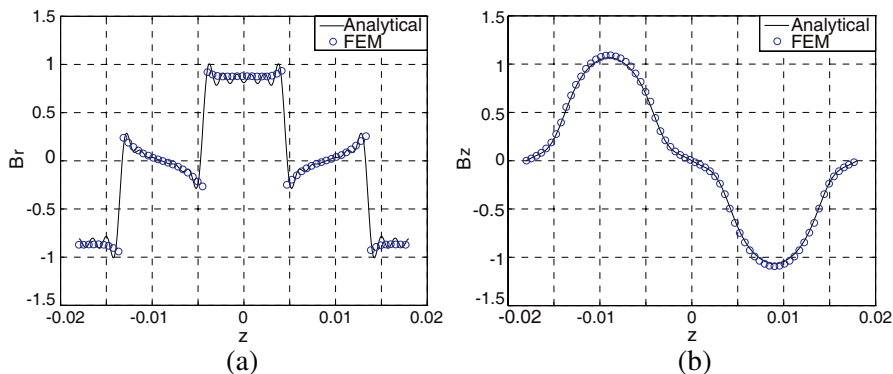
Figure 9. Field variation at the center of internal magnet area. (a) Variation of B_r. (b) Variation of B_z.
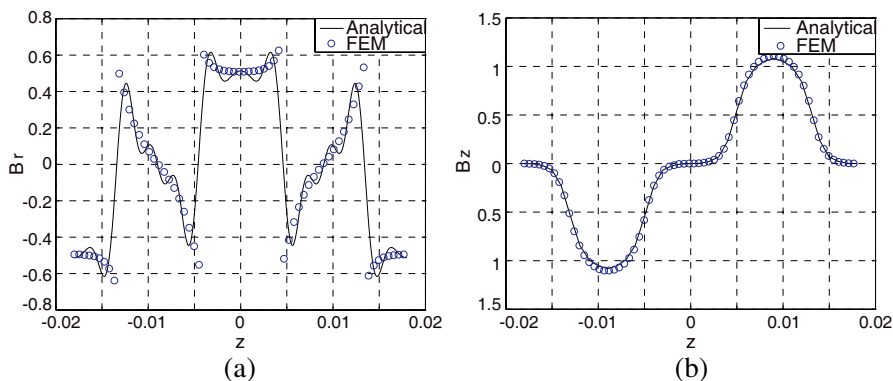
Figure 10. Field variation at the external magnet area. (a) Variation of B_r. (b) Variation of B_z.

area due to a decreasing section crossed by constant flux lines. The analytical results fit with the finite element results well. The difference is mainly caused by the simplification of models and FEM meshing.

6. CONCLUSION

A novel dual Halbach magnet array is proposed in this paper for the development of tubular linear machines. It helps to improve the radial flux, and reduce the axial flux. The 3D magnetic field distribution is formulated analytically based on Laplace's and Poisson's equations. Numerical computation of magnetic field is conducted with FEM method. It shows that the analytical model fits with the numerical result closely. A research prototype and an automatic apparatus are developed for experimental purpose. The experimental result validates the analytical magnetic field model well. The analytical model in this paper can be used for design optimization and control implementation of tubular electromagnetic linear machines. The proposed dual Halbach array can also be utilized for rotary machines.

ACKNOWLEDGMENT

REFERENCES

1. Stumberger, G., M. T. Aydemir, D. Zarko, and T. A. Lipo, "Design of a linear bulk superconductor magnet synchronous motor for electromagnetic aircraft launch systems," *IEEE Transactions on Applied Superconductivity*, Vol. 14, No. 1, 54–62, 2004.

2. Kou, B. Q., X. Z. Huang, H. X. Wu, and L. Y. Li, "Thrust and thermal characteristics of electromagnetic launcher based on permanent magnet linear synchronous motors," *IEEE Transactions on Magnetics*, Vol. 45, No. 1, 358–362, 2009.

3. Thornton, R., M. T. Thompson, B. M. Perreault, and J. R. Fang, "Linear motor powered transportation," *Proceedings of the IEEE*, Vol. 97, No. 11, 1754–1757, 2009.

4. Yan L. G., "The linear motor powered transportation development and application in China," *Proceedings of the IEEE*, Vol. 97, No. 11, 1872–1880, 2009.

5. Yamada, H., M. Yamaguchi, M. Karita, Y. Matsuura, and

S. Fukunaga, "Acute animal experiment using a linear motor-driven total artificial heart," *IEEE Translation Journal on Magnetics in Japan*, Vol. 9, No. 6, 90–97, 1994.

6. Yamada, H., M. Yamaguchi, K. Kobayashi, Y. Matsuura, and H. Takano, "Development and test of a linear motor-driven total artificial heart," *IEEE Engineering in Medicine and Biology Magazine*, Vol. 14, No. 11, 84–90, 1995.

7. Mohammadpour, A., A. Gandhi, and L. Parsa, "Winding factor calculation for analysis of back EMF waveform in air-core permanent magnet linear synchronous motors," *IET Electric Power Applications*, Vol. 6, No. 5, 253–259, 2012.

8. Wang, J. B. and D. Howe, "Design optimization of radially magnetized, iron-cored, tubular permanent-magnet machines and drive systems," *IEEE Transactions on Magnetics*, Vol. 40, No. 5, 3262–3277, 2004.

9. Mahmoudi, A., N. A. Rahim, and W. P. Hew, "Axial-flux permanent-magnet motor design for electric vehicle direct drive using sizing equation and finite element analysis," *Progress In Electromagnetics Research*, Vol. 122, 467–496, 2012.

10. Wang, J., G. W. Jewell, and D. Howe, "A general framework for the analysis and design of tubular linear permanent magnet machines," *IEEE Transactions on Magnetics*, Vol. 35, No. 3, 1986–2000, 1999.

11. Fang, J. R., D. B. Montgomery, and L. Roderick, "A novel mag pipe pipeline transportation system using linear motor drives," *Proceedings of the IEEE*, Vol. 97, No. 11, 1848–1855, 2009.

12. Gurol, H., "General atomics linear motor applications: Moving towards deployment," *Proceedings of the IEEE*, Vol. 97, No. 11, 1864–1871, 2009.

13. Torkaman, H. and E. Afjei, "Magnetostatic field analysis regarding the effcts of dynamic eccentricity in switched reluctance motor," *Progress In Electromagnetics Research M*, Vol. 8, 163–180, 2009.

14. Torkaman, H. and E. Afjei, "Comparison of two types of dual layer generator in field assisted mode utilizing 3D-FEM and experimental verification," *Progress In Electromagnetics Research B*, Vol. 23, 293–309, 2010.

15. Torkaman, H. and E. Afjei, "Comparison of three novel types of two-phase switched reluctance motors using finite element method," *Progress In Electromagnetics Research*, Vol. 125, 151–164, 2012.

16. Jian, L. and K.-T. Chau, "Design and analysis of a magnetic-geared electronic-continuously variable transmission system using finite element method," *Progress In Electromagnetics Research*, Vol. 107, 47–61, 2010.

17. Touati, S., R. Ibtiouen, O. Touhami, and A. Djerdir, "Experimental investigation and optimization of permanent magnet motor based on coupling boundary element method with permeances network," *Progress In Electromagnetics Research*, Vol. 111, 71–90, 2011.

18. Lecointe, J. P., B. Cassoret, and J.-F. Brudny, "Distinction of toothing and saturation effects on magnetic noise of induction motors," *Progress In Electromagnetics Research*, Vol. 112, 125–137, 2011.

19. Zhao, W., M. Cheng, R. Cao, and J. Ji, "Experimental comparison of remedial single-channel operations for redundant flux-switching permanent-magnet motor drive," *Progress In Electromagnetics Research*, Vol. 123, 189–204, 2012.

20. Mahmoudi, A., S. Kahourzade, N. A. Rahim, and W. P. Hew, "Improvement to performance of solid-rotor-ringed line-start axial-flux permanent-magnet motor," *Progress In Electromagnetics Research*, Vol. 124, 383–404, 2012.

21. Musolino, A., R. Rizzo, and E. Tripodi, "Tubular linear induction machine as a fast actuator: Analysis and design criteria," *Progress In Electromagnetics Research*, Vol. 132, 603–619, 2012.

22. Matyas, A. R., K. A. Biro, and D. Fodorean, "Multi-phase synchronous motor solution for steering applications," *Progress In Electromagnetics Research*, Vol. 131, 63–80, 2012.

23. Youn, H. K., S. J. Chang, K. Sol, D. C. Yon, and L. Ju, "Analysis of hybrid stepping motor using 3D equivalent magnetic circuit network method based on trapezoidal element," *Journal of Applied Physics*, Vol. 91, No. 10, 8311–8313, 2002.

24. Amrhein, M. and P. T. Krein, "Induction machine modeling approach based on 3-D magnetic equivalent circuit framework," *IEEE Transactions on Energy Conversion*, Vol. 25, No. 2, 339–347, 2010.

25. Liu, C. and K.-T. Chau, "Electromagnetic design and analysis of double-rotor flux-modulated permanent-magnet machines," *Progress In Electromagnetics Research*, Vol. 131, 81–97, 2012.

26. The Wolfram functions site, 2012, http://functions.wolfram.com/Bessel-TypeFunctions/StruveL/introductions/Struves/01/.